**SCIENCE CHINA**
Information Sciences

• **Supplementary File** •

# Experimental realization of deterministic joint remote preparation of an arbitrary two-qubit pure state via GHZ states

Nachuan Li[1], Lu Xu[2] & Jin-Ming Liu[1*]

[1]*State Key Laboratory of Precision Spectroscopy, School of Physics and Electronic Science, East China Normal University, Shanghai* 200241*, China;*
[2]*Hefei Origin Quantum Computing Technology Co., Ltd., Hefei* 230088*, China*

## Appendix A Introduction

Applying quantum mechanics in computer science and information theory has spawned some hot research areas in recent years. It is well accepted that in the field of quantum information, quantum teleportation (QT) [1], proposed originally by Bennett *et al*. in 1993, is one of the most prominent quantum communication protocols by means of the shared entanglement resource between the sender and the receiver. Subsequently, Lo [2], Pati [3], and Bennett et al. [4] presented a similar protocol called remote state preparation (RSP), i.e., teleportation of a known state, in which the sender has complete knowledge of the initial state while the receiver does not. Similar to QT, to achieve the task of RSP, the sender and the receiver require sharing an entangled channel in advance with the assistance of some classical information. But in contrast to QT, in RSP it is possible to exhibit a substantial trade-off between the required entanglement and the cost of classical communication. Due to the remarkable advantages, the RSP has been extensively studied in discrete variable systems theoretically [5–13] and experimentally [14–23]. Moreover, discrete variable RSP schemes have been generalized to the cases of continuous variable RSP [24–27]. Further, there can be multiple senders, rather than one, who share the information of the initial state. A novel kind of RSP with multiple senders is called joint RSP (JRSP), first proposed by Xia *et al*. [28]. Soon after, the two-sender JRSP protocols using a single GHZ-like state and a pair of EPR-like states were studied [29], where the shared quantum channel cannot necessarily be maximally entangled. Since then, the study of JRSP has begun to develop rapidly. Many schemes of remotely preparing two-qubit states [30–34], three-qubit states [35–38], four-qubit states [39,40], and multi-qubit states [41] have been examined in succession. Besides, remote preparation of an arbitrary single-photon pure state is designed using a linear optics system [42].

Generally, quantum systems inevitably interact with their surroundings, losing their mysterious quantum properties. Thus, considering the JRSP protocol in noise environments is of great significance. As we know, a master equation can describe the dynamic behavior of JRSP in a dissipative environment. Chen *et al*. [43] investigated the influence of Pauli noises on the deterministic JRSP. Li *et al*. [44] showed that the average fidelity of JRSP of an arbitrary two-qubit state decreases gradually to a stable value with a dampened revival amplitude in the non-Markovian regime. Furthermore, Gu *et al*. [45] investigated a bidirectional controlled remote preparation of a single-qubit state in dissipative environments and adopted two methods of weak measurement reversal and detuning modulation to improve the average fidelity. On the other hand, by using the Kraus operator description [46], the effects of various types of noises on different JRSP processes have been studied by many researchers. Wang *et al*. [47] and Qian *et al*. [48] investigated the JRSP of any single-qubit state in noise environments. Adepoju *et al*. [49] reported the effect of five different noises on the deterministic JRSP of two-qubit equatorial states, using tripartite GHZ states as the entangled resource. In addition, the effects of various noise environments on other JRSP schemes of two-qubit states [50–52] and mixed states [53] were investigated.

Currently, many cloud quantum computing platforms are accessible and conveniently used for research, application exploration, and education. Some platforms based on superconducting processors have been launched for online users, such as IBM Quantum Experience, Rigetti Cloud Services and ScQ Cloud, where a series of theoretical schemes in the field of quantum communication [54,55], quantum fault tolerance [56–58], entangled state generation [59,60], distinguishing unitary gates [61], and so forth [62–68], have been performed and verified. Nevertheless, to our knowledge, there have not been verifications of the JRSP protocol utilizing quantum platforms. To verify the feasibility of the JRSP protocol [35], we use Origin Quantum Cloud for the experimental realization and noise simulation. We analyze the influence of four environmental noises on the average fidelity of the JRSP process using analytical derivation and numerical calculations.

* Corresponding author (email: jmliu@phy.ecnu.edu.cn)

**Table B1** The corresponding relation among Alice's measurement results for qubits 0 and 1 ($M_A$), unitary operations for qubits 2 and 3 ($U_{23}$), and unitary operations for qubits 4 and 5 ($U_{45}$), while the corresponding relation between Bob's measurement results for qubits 2 and 3 ($M_B$) and unitary operations for qubits 4 and 5 ($U_{45}$).

| $M_A$ | $U_{23}$ | $U_{45}$ | $M_B$ | $U_{45}$ |
|---|---|---|---|---|
| $\vert\varphi_0\rangle_{01}$ | $I_2 \otimes I_3$ | $I_4 \otimes I_5$ | $\vert\phi_0\rangle_{23}$ | $I_4 \otimes I_5$ |
| $\vert\varphi_1\rangle_{01}$ | $I_2 \otimes (\mathrm{i}\sigma_y)_3$ | $(\sigma_x)_4 \otimes I_5$ | $\vert\phi_1\rangle_{23}$ | $(\sigma_z)_4 \otimes I_5$ |
| $\vert\varphi_2\rangle_{01}$ | $(\sigma_z)_2 \otimes (\mathrm{i}\sigma_y)_3$ | $I_4 \otimes (\sigma_x)_5$ | $\vert\phi_2\rangle_{23}$ | $I_4 \otimes (\sigma_z)_5$ |
| $\vert\varphi_3\rangle_{01}$ | $(\sigma_x)_2 \otimes (\mathrm{i}\sigma_y)_3$ | $(\sigma_x)_4 \otimes (\sigma_x)_5$ | $\vert\phi_3\rangle_{23}$ | $(\sigma_z)_4 \otimes (\sigma_z)_5$ |

Additionally, we examine the JRSP of two unique initial states on the Origin Noise Quantum Virtual Machine (NQVM) platform in four noise environments. Specifically, we find that replacing the Hadamard gates in the GHZ state preparation circuit with parameterized unitary operations can enhance the fidelity of remotely preparing certain states in the presence of phase-flip and amplitude-damping noises. Our work could shed some light on the physical realization of more complex quantum communication tasks.

This paper is organized as follows. We briefly review the deterministic JRSP protocol of an arbitrary two-qubit pure state via two GHZ states in Appendix B. Implementation of the JRSP protocol on Origin Wuyuan Chip is described in Appendix C. Appendix D is devoted to the fidelities of the protocol in several noise environments. Besides, we verify the theoretical fidelities by remotely preparing two unique states on the NQVM and propose a method to improve the fidelities of the JRSP process in Appendix E. Finally, we end our paper with a conclusion in Appendix F. The Detailed data is presented in Appendixes G-H.

## Appendix B Review of the deterministic joint remote preparation of an arbitrary two-qubit pure state via GHZ states

In this appendix, we briefly review the deterministic joint remote preparation protocol of an arbitrary two-qubit pure state via GHZ states [35]. Assume there are three valid parties in the protocol, where Alice and Bob are the senders, and Charlie is the receiver. Alice and Bob wish to jointly prepare an arbitrary two-qubit pure state in the location of Charlie. The initial state of being remotely prepared [12] can be expressed as

$$|\Psi\rangle = \alpha_0|00\rangle + \alpha_1 \mathrm{e}^{\mathrm{i}\lambda_1}|01\rangle + \alpha_2 \mathrm{e}^{\mathrm{i}\lambda_2}|10\rangle + \alpha_3 \mathrm{e}^{\mathrm{i}\lambda_3}|11\rangle, \tag{B1}$$

where the real parameters $\lambda_k \in [0, 2\pi]$ $(k = 1, 2, 3)$, and $\alpha_j \geqslant 0$ $(j = 0, 1, 2, 3)$ meet the normalization condition $\sum_{j=0}^{3} \alpha_j^2 = 1$. We assume that Alice and Bob know the parameters $\alpha_j$ and $\lambda_k$, respectively. Thus, the two senders have complete knowledge of the state $|\Psi\rangle$ through collaboration. To achieve the preparation, the three parties need to cooperate and take the following steps.

**Step 1** Alice, Bob, and Charlie initially share two GHZ states as their quantum channel

$$\begin{aligned} |\Phi\rangle_{024} &= \frac{1}{\sqrt{2}}(|000\rangle_{024} + |111\rangle_{024}), \\ |\Phi\rangle_{135} &= \frac{1}{\sqrt{2}}(|000\rangle_{135} + |111\rangle_{135}), \end{aligned} \tag{B2}$$

of which particles 0 and 1 belong to Alice, particles 2 and 3 belong to Bob, and particles 4 and 5 belong to Charlie. To help Charlie remotely prepare the state $|\Psi\rangle$, Alice first carries out a projective measurement (PM1) on her particles 0 and 1 according to her knowledge. She chooses a set of orthonormal vectors $\{|\varphi_r\rangle_{01} = U_1(r)|\varphi_0\rangle_{01}, (r = 0, 1, 2, 3)\}$ as measurement basis with $U_1(0) = I_0 \otimes I_1$, $U_1(1) = I_0 \otimes (-\mathrm{i}\sigma_y)_1$, $U_1(2) = (-\mathrm{i}\sigma_y)_0 \otimes (\sigma_z)_1$, $U_1(3) = (-\mathrm{i}\sigma_y)_0 \otimes (\sigma_x)_1$, and $|\varphi_0\rangle_{01} = (\alpha_0|00\rangle + \alpha_1|01\rangle + \alpha_2|10\rangle + \alpha_3|11\rangle)_{01}$, where $I$ is an identity operation, and $\sigma_x$, $\sigma_y$, $\sigma_z$ are Pauli operations. Then Alice transmits her measurement result to Bob and Charlie through classical channels.

**Step 2** Bob does not measure his particles right after he receives the message. According to Alice's measurement result, Bob performs corresponding local unitary operations on particles 2 and 3. Subsequently, he implements a projective measurement (PM2) on his particles under the basis $\{|\phi_r\rangle_{23} = U_2(r')|\phi_0\rangle_{23}, (r' = 0, 1, 2, 3)\}$ with $U_2(0) = I_2 \otimes I_3$, $U_2(1) = I_2 \otimes (\sigma_z)_3$, $U_3(2) = (\sigma_z)_2 \otimes I_3$, $U_2(3) = (\sigma_z)_2 \otimes (\sigma_z)_3$, and $|\phi_0\rangle_{23} = \frac{1}{2}(|00\rangle + \mathrm{e}^{-\mathrm{i}\lambda_1}|01\rangle + \mathrm{e}^{-\mathrm{i}\lambda_2}|10\rangle + \mathrm{e}^{-\mathrm{i}\lambda_3}|11\rangle)_{23}$, and then informs Charlie of his measurement outcome.

**Step 3** Based on the classical messages from Alice and Bob, Charlie performs corresponding local unitary operations on particles 4 and 5. Finally, the initial state $|\Psi\rangle$ can be successfully restored at Charlie's side with unit probability.

During the JRSP process, the relation between Alice's and Bob's measurement results and the corresponding unitary operations performed by Bob and Charlie is shown in Table B1. Note that Chen *et al.* [43] have constructed an optimized quantum circuit of the JRSP protocol with a set of single- and two-qubit logical gates. To execute the above protocol on Origin Quantum Cloud, we adjust the order of some quantum gates in Chen's circuit. This is necessary because Origin Quantum uses a specific ordering where the $n$-th qubit is situated on the left-hand side of the tensor product, which is different from the convention found in many physics textbooks. In this way, our designed quantum circuit is shown in Figure B1, where the dot '•' denotes the control qubit while the cross '⊕' denotes the target qubits. Here, the two-qubit

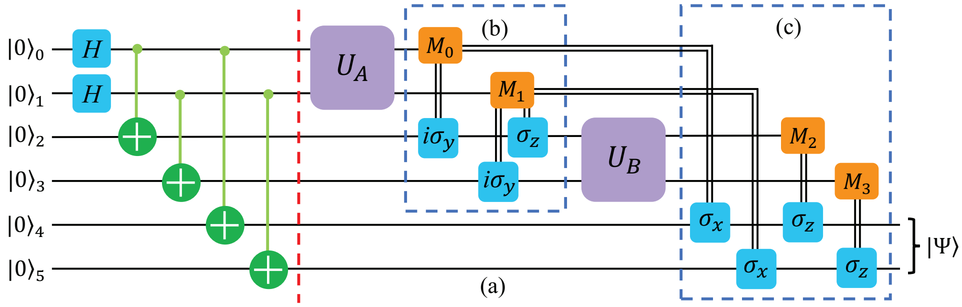


**Figure B1** (Color online) (a) Quantum circuits for the deterministic JRSP of an arbitrary two-qubit pure state via GHZ states. The top two qubits belong to Alice, the two in the middle are owned by Bob, and the others belong to Charlie. Circuits before the red dashed line are designed to generate two GHZ states. (b) The unitary operations performed by Bob depend on Alice's classical message. (c) The unitary operations that Charlie implements on particles 4 and 5, according to messages from Alice and Bob. $M_q$ ($q \in \{0, 1, 2, 3\}$) denotes the single-qubit projective measurement on particle $q$, and the double line represents the classical information.

unitary amplitude operation $U_A$ and phase operation $U_B$ take the following respective forms

$$U_A = \begin{pmatrix} \alpha_0 & \alpha_1 & \alpha_2 & \alpha_3 \\ \alpha_1 & -\alpha_0 & \alpha_3 & -\alpha_2 \\ \alpha_2 & -\alpha_3 & -\alpha_0 & \alpha_1 \\ \alpha_3 & \alpha_2 & -\alpha_1 & -\alpha_0 \end{pmatrix}, \tag{B3}$$

$$U_B = \frac{1}{2}\begin{pmatrix} 1 & \mathrm{e}^{\mathrm{i}\lambda_1} & \mathrm{e}^{\mathrm{i}\lambda_2} & \mathrm{e}^{\mathrm{i}\lambda_3} \\ 1 & -\mathrm{e}^{\mathrm{i}\lambda_1} & \mathrm{e}^{\mathrm{i}\lambda_2} & -\mathrm{e}^{\mathrm{i}\lambda_3} \\ 1 & \mathrm{e}^{\mathrm{i}\lambda_1} & -\mathrm{e}^{\mathrm{i}\lambda_2} & -\mathrm{e}^{\mathrm{i}\lambda_3} \\ 1 & -\mathrm{e}^{\mathrm{i}\lambda_1} & -\mathrm{e}^{\mathrm{i}\lambda_2} & \mathrm{e}^{\mathrm{i}\lambda_3} \end{pmatrix}. \tag{B4}$$

## Appendix C Experimental realization of deterministic joint remote preparation of an arbitrary two-qubit pure state via GHZ states

In this appendix, we describe how to perform the above deterministic JRSP protocol on the Origin Wuyuan 6-qubit chip with a superconducting system. We select the following six different initial states [69] to be remotely prepared

$$\begin{aligned} |\Psi_1\rangle &= |00\rangle, \\ |\Psi_2\rangle &= |11\rangle, \\ |\Psi_3\rangle &= \frac{1}{2}(|0\rangle + |1\rangle)(|0\rangle + |1\rangle), \\ |\Psi_4\rangle &= \frac{1}{2}(|0\rangle + \mathrm{i}|1\rangle)(|0\rangle + \mathrm{i}|1\rangle), \\ |\Psi_5\rangle &= \frac{1}{\sqrt{2}}(|00\rangle + |11\rangle), \\ |\Psi_6\rangle &= \frac{1}{\sqrt{2}}(|01\rangle - |10\rangle), \end{aligned} \tag{C1}$$

which can be grouped into three categories: $|\Psi_1\rangle$ and $|\Psi_2\rangle$ are product states of the two qubits in the computational basis; $|\Psi_3\rangle$ and $|\Psi_4\rangle$ are product states of the two qubits in the superposition basis; $|\Psi_5\rangle$ and $|\Psi_6\rangle$ are two of the four Bell states.

The quantum circuit of remotely preparing state $|\Psi_1\rangle$ on the Origin Quantum Cloud is shown in Figure C1 as an example. Here, Alice's unitary transformation $U_A$ and Bob's unitary transformation $U_B$ are decomposed with a combination of single-qubit and CNOT gates. Moreover, the unitary operations RY, RZ, and Controlled-Z are expressed as

$$\mathrm{RY} = \begin{pmatrix} \cos(\frac{\xi}{2}) & -\sin(\frac{\xi}{2}) \\ \sin(\frac{\xi}{2}) & \cos(\frac{\xi}{2}) \end{pmatrix}, \quad \mathrm{RZ} = \begin{pmatrix} \mathrm{e}^{-\mathrm{i}\frac{\delta}{2}} & 0 \\ 0 & \mathrm{e}^{\mathrm{i}\frac{\delta}{2}} \end{pmatrix}, \quad \text{Controlled-Z} = \begin{pmatrix} 1 & 0 & 0 & 0 \\ 0 & 1 & 0 & 0 \\ 0 & 0 & 1 & 0 \\ 0 & 0 & 0 & -1 \end{pmatrix}. \tag{C2}$$

We also run our circuits of the above six states on the Origin quantum simulator to compare the probability distribution between the real device (Origin 6-qubit chip) and the virtual quantum simulator. Both with 8192 shots, as shown in Figure C2, the probability distribution of each state of the real device is similar to the case of the simulator. However, why is there a discrepancy? Due to the unavoidably noise environment surrounding the real chip, decoherence in the quantum

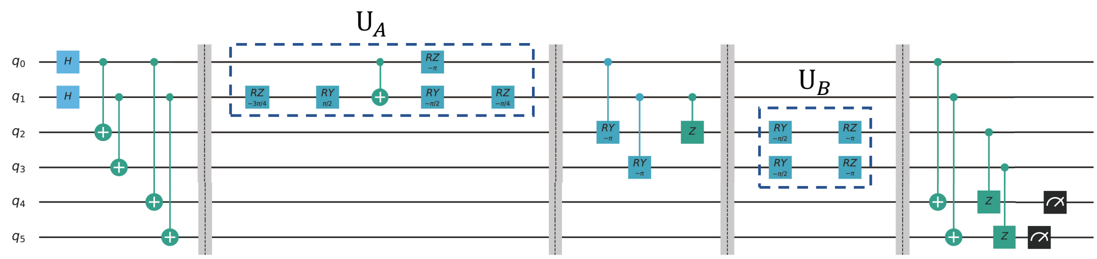


**Figure C1** (Color online) The quantum circuit of remotely preparing state $|\Psi_1\rangle$ on the Origin Quantum Cloud, where each of six qubits is initially prepared in the state $|0\rangle$, and each numerical value in the logical gate represents the corresponding gate parameter.

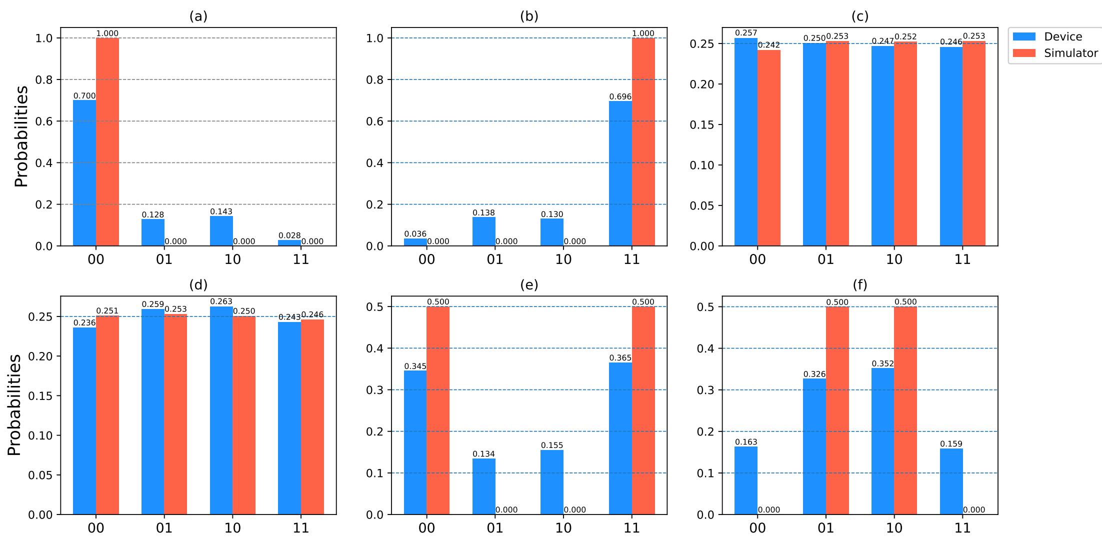


**Figure C2** (Color online) Histogram of the probability distribution obtained by the Origin 6-qubit chip and the Origin simulator for remotely preparing (a)-(f) $|\Psi_1\rangle - |\Psi_6\rangle$.

channel, state preparation errors, and gate errors, all these factors play important roles in reducing the fidelity of our JRSP protocol.

Fidelity is defined to calculate the distance between quantum states, which we use to show how well the initial state is prepared remotely. The fidelity is given by

$$F(\rho^T, \rho^E) = \left( tr\sqrt{\sqrt{\rho^T}\rho^E\sqrt{\rho^T}} \right)^2, \tag{C3}$$

where $\rho^T$ is the theoretical density matrix, and $\rho^E$ is the experimental one. Here, we take $|\Psi_3\rangle$ as an example whose $\rho^T$ is obtained as

$$\rho^T = \frac{1}{4}\begin{pmatrix} 1 & 1 & 1 & 1 \\ 1 & 1 & 1 & 1 \\ 1 & 1 & 1 & 1 \\ 1 & 1 & 1 & 1 \end{pmatrix}. \tag{C4}$$

The experimental density matrix $\rho^E$ for two-qubit states is given by

$$\rho^E = \frac{1}{4}\sum_{j_1,j_2=0}^{3} T_{j_1 j_2}(\sigma_{j_1} \otimes \sigma_{j_2}), \tag{C5}$$

where $\sigma_j$ $(j = 0,1,2,3)$ correspond to the identity matrix $I$ and $\sigma_x$, $\sigma_y$, $\sigma_z$ Pauli matrices, respectively, and $T_{j_1 j_2} = S_{j_1} \times S_{j_2}$. $S_{j_1}$ and $S_{j_2}$ are the Stokes parameters expressed as $S_0 = P_{|0I\rangle} + P_{|1I\rangle}$, $S_1 = P_{|0X\rangle} - P_{|1X\rangle}$, $S_2 = P_{|0Y\rangle} - P_{|1Y\rangle}$, and $S_3 = P_{|0Z\rangle} - P_{|1Z\rangle}$, where $P_{|0j\rangle}$ and $P_{|1j\rangle}$ represent the probability of the qubit being in $|0\rangle$ and $|1\rangle$, respectively, when measured in $j$ basis.

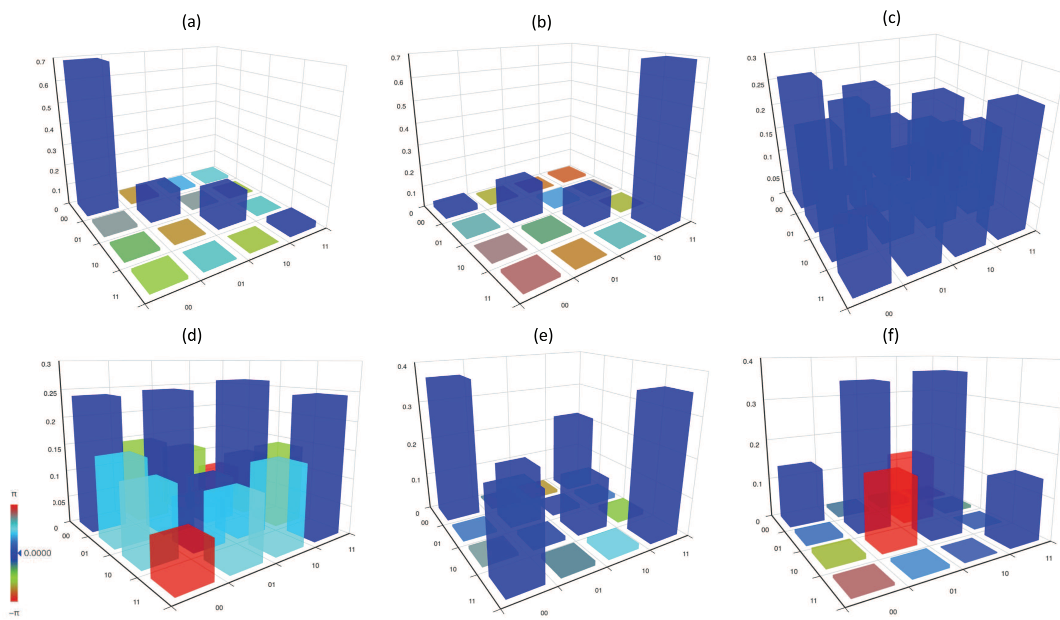


**Figure C3** (Color online) Density matrices of remote preparation of (a)-(f) $|\Psi_1\rangle - |\Psi_6\rangle$ by quantum state tomography.

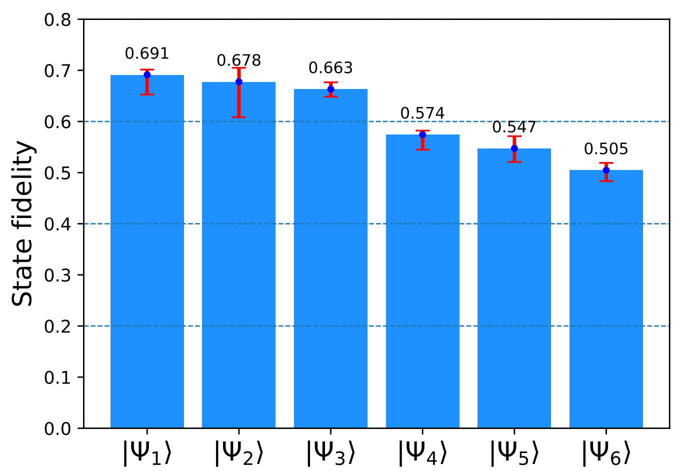


**Figure C4** (Color online) Experimental results of remote preparation of six initial states using the Origin Wuyuan 6-qubit chip. Error bars (marked in red) represent the deviation from average fidelities shown in the blue dots since the JRSP protocol is implemented ten times to gain the fidelities for each initial state.

The results of quantum state tomography are shown in Figure C3. For example, from the data obtained by the Origin 6-qubit chip (Figure C3(c)), the experimental density matrix of $|\Psi_3\rangle$ can be written as follows

$$\rho^E = \begin{pmatrix} 0.2458 & 0.1807 & 0.1338 & 0.0937 \\ 0.1807 & 0.2539 & 0.1001 & 0.1528 \\ 0.1338 & 0.1001 & 0.2696 & 0.1921 \\ 0.0937 & 0.1528 & 0.1921 & 0.2549 \end{pmatrix} + \mathrm{i} \begin{pmatrix} 0 & -0.0013 & -0.0010 & -0.0033 \\ 0.0013 & 0 & 0.0066 & -0.0008 \\ 0.0010 & -0.0066 & 0 & -0.0096 \\ 0.0033 & 0.0008 & 0.0096 & 0 \end{pmatrix}. \tag{C6}$$

The fidelity between the theoretical density matrix of Eq. (C4) and the experimental one of Eq. (C6) is 0.6766. The density matrices and state fidelities of the other five remotely prepared states are shown in the Appendix G. We run the Origin Wuyuan 6-qubit chip ten times for each of the six initial states to calculate the mean fidelity. Despite the experimental noise, the average measured fidelities (Figure C4) of the six states are all well above 0.40 —— the classical limit, defined in Ref. [69] as the optimal mean fidelity of state estimation of a two-qubit system with single copy [70]. Significantly, the mean experimental fidelity of JRSP of $|\Psi_3\rangle$ is about 0.19 more than that of teleportation of $|\Psi_3\rangle$ in [54], which is only 0.4919.

## Appendix D Deterministic joint remote preparation of an arbitrary two-qubit pure state in noise environments

In natural quantum systems, there are often inevitable errors due to the physical properties of qubits themselves. In order to better simulate these errors in the quantum system, we use the NQVM on Origin Quantum Cloud. The simulation of the virtual machine with noise is closer to the natural quantum systems, which makes the protocols more applicable. Under the assumption of Markov and Born approximations, and after tracing over the environmental degrees of freedom, how a system couples with an environment can be described in terms of the operator-sum of Kraus operators.

From Figure B1, the input qubits of the quantum circuit are all set to state $|0\rangle$. The output states of the GHZ state preparation process and our whole JRSP protocol in particles 4 and 5 become

$$\begin{aligned}\rho_{GHZ} &= U_{GHZ}(\rho_{in})U_{GHZ}^{\dagger},\\ \rho_{out} &= Tr_{0123}\{U_{JRSP}(\rho_{GHZ})U_{JRSP}^{\dagger}\},\end{aligned} \tag{D1}$$

respectively, where $\rho_{in} = |0\rangle^{\otimes 6}$ and $Tr_{0123}$ is the partial trace over qubits 0, 1, 2, and 3. The unitary operation $U_{GHZ}$ and $U_{JRSP}$ are given by

$$U_{GHZ} = CX_{1\to 5}CX_{0\to 4}CX_{1\to 3}CX_{0\to 2}H_1H_0, \tag{D2}$$

$$U_{JRSP} = CZ_{3\to 5}CZ_{2\to 4}CX_{1\to 5}CX_{0\to 4}(U_B)_{23}CZ_{1\to 2}CiY_{1\to 3}CiY_{0\to 2}(U_A)_{01}, \tag{D3}$$

respectively. Here, $H_p(p = 0, 1)$ represents the Hadamard gate on qubit $p$, $CX_{m\to n}, CiY_{m\to n}$, and $CZ_{m\to n}$ are the controlled $X$, $iY$, and $Z$ gates where qubit $n$ is controlled by qubit $m$. If the control qubit $m$ is in the state $|1\rangle$, the controlled gate performs a corresponding unitary operation on the target qubit $n$, while the qubit $n$ keeps invariant when the qubit $m$ is in the state $|0\rangle$.

In the following, we only consider the preparation process of two GHZ states subjected to the Pauli noises. Four typical kinds of noise often encountered in reality are phase-flip (P), bit-flip (B), amplitude-damping (A), and depolarizing (D), which can be described by Kraus representation. The transformation of the density matrix in the noise environment can be written as

$$\rho \to \mathcal{E}(\rho) = \sum_k E_k \rho E_k^{\dagger}, \tag{D4}$$

where $E_k$ is the Kraus operator for different noise types. Suppose that each of the qubits independently suffers from the same kind of noise, then the Kraus operator of the double-qubit noise model has a corresponding relationship with the single-qubit noise model. If the Kraus operators of single-qubit noise are $E_0$ and $E_1$, those of double-qubit noise are $E_0 \otimes E_0$, $E_0 \otimes E_1$, $E_1 \otimes E_0$, and $E_1 \otimes E_1$. The single- and double-qubit noise acts on every single and controlled gate, respectively.

(i) At first, we consider the situation that all operators in $U_{GHZ}$ are subjected to phase-flip noise, whose Kraus operators take the form of

$$E_0 = \begin{pmatrix} \sqrt{1-p} & 0 \\ 0 & \sqrt{1-p} \end{pmatrix}, \qquad E_1 = \begin{pmatrix} \sqrt{p} & 0 \\ 0 & -\sqrt{p} \end{pmatrix}, \tag{D5}$$

where $p$ describes the probability of the qubit coupling with its environment. Calculated by Eq. (C6) in the phase-flip noise environment, the density matrix of the output state consisting of particles 4 and 5 can be derived as

$$\tilde{\rho}_{45} = \begin{pmatrix} \alpha_0^2 & \mathrm{e}^{-\mathrm{i}\lambda_1}(1-2p)^5\alpha_0\alpha_1 & \mathrm{e}^{-\mathrm{i}\lambda_2}(1-2p)^5\alpha_0\alpha_2 & \mathrm{e}^{-\mathrm{i}\lambda_3}(1-2p)^{10}\alpha_0\alpha_3 \\ \mathrm{e}^{\mathrm{i}\lambda_1}(1-2p)^5\alpha_0\alpha_1 & \alpha_1^2 & \mathrm{e}^{\mathrm{i}(\lambda_1-\lambda_2)}(1-2p)^{10}\alpha_1\alpha_2 & \mathrm{e}^{\mathrm{i}(\lambda_1-\lambda_3)}(1-2p)^5\alpha_1\alpha_3 \\ \mathrm{e}^{\mathrm{i}\lambda_2}(1-2p)^5\alpha_0\alpha_2 & \mathrm{e}^{\mathrm{i}(\lambda_2-\lambda_1)}(1-2p)^{10}\alpha_1\alpha_2 & \alpha_2^2 & \mathrm{e}^{\mathrm{i}(\lambda_2-\lambda_3)}(1-2p)^5\alpha_2\alpha_3 \\ \mathrm{e}^{\mathrm{i}\lambda_3}(1-2p)^{10}\alpha_0\alpha_3 & \mathrm{e}^{\mathrm{i}(\lambda_3+\lambda_1)}(1-2p)^5\alpha_1\alpha_3 & \mathrm{e}^{\mathrm{i}(\lambda_3-\lambda_2)}(1-2p)^5\alpha_2\alpha_3 & \alpha_3^2 \end{pmatrix}. \tag{D6}$$

According to Eq. (C3), we obtain the fidelity

$$F^P = \alpha_0^4 + \alpha_1^4 + \alpha_2^4 + \alpha_3^4 + 2(1-2p)^5(\alpha_0^2\alpha_1^2 + \alpha_0^2\alpha_2^2 + \alpha_1^2\alpha_3^2 + \alpha_2^2\alpha_3^2) + 2(1-2p)^{10}(\alpha_1^2\alpha_2^2 + \alpha_0^2\alpha_3^2). \tag{D7}$$

The fidelity $F^P$ depends only on the amplitude information of the initial state to be remotely prepared but not on the phase information of the state $|\Psi\rangle$. And since the input state is an arbitrary pure state of two qubits, it is more important to analyze the average fidelity of all possible input states, which is defined as [43]

$$F_{av} = \left(\int_0^{2\pi}\int_0^{2\pi}\int_0^{2\pi} d\lambda_1 d\lambda_2 d\lambda_3 \int_0^{\pi}\int_0^{\pi}\int_0^{\pi} d\alpha d\beta d\delta\ F \sin\alpha \sin\beta \sin\delta\right)/(64\pi^3), \tag{D8}$$

where $\alpha_0 = \cos\frac{\alpha}{2}\cos\frac{\beta}{2}$, $\alpha_1 = \cos\frac{\alpha}{2}\sin\frac{\beta}{2}$, $\alpha_2 = \sin\frac{\alpha}{2}\cos\frac{\delta}{2}$, $\alpha_3 = \sin\frac{\alpha}{2}\sin\frac{\delta}{2}$, and $\alpha, \beta, \delta \in [0, \pi]$. Substituting Eq. (D7) into Eq. (D8), the corresponding average fidelity can be calculated as

$$F_{av}^P = \frac{1}{9}p\{4p\,[2p\,(p\,(2p-5)+5)-5]+5\}\{6p\,[4p\,(2p\,(p\,(2p-5)+5)-5)+5]-13\}+1. \tag{D9}$$

(ii) Next, we consider the case when every gate of the GHZ states preparation process is affected by the bit-flip noise. In this case, the Kraus operators take the form of

$$E_0 = \begin{pmatrix} \sqrt{1-p} & 0 \\ 0 & \sqrt{1-p} \end{pmatrix}, \qquad E_1 = \begin{pmatrix} 0 & \sqrt{p} \\ \sqrt{p} & 0 \end{pmatrix}. \tag{D10}$$

The fidelity $F^B$ is calculated as

$$\begin{aligned}F^B =&8\left(\alpha_1^2\alpha_2^2+\alpha_0^2\alpha_3^2\right)p^2(p-1)^2-4\left(\alpha_1^2+\alpha_2^2\right)\left(\alpha_0^2+\alpha_3^2\right)p\left(2p^2-2p+1\right)(p-1)\\&+\left(\alpha_0^4+\alpha_1^4+\alpha_2^4+\alpha_3^4\right)\left(2p^2-2p+1\right)^2+\alpha_0\alpha_1\alpha_2\alpha_3p(p-1)\{4\mathrm{i}\left(2p^2-2p+1\right)\\&\times\sin\left(\lambda_1-\lambda_2-\lambda_3\right)-16p\left(4p^2-6p+3\right)\cos\left(\lambda_1-\lambda_2\right)\cos\left(\lambda_3\right)\cos^2[\frac{1}{2}\left(\lambda_1+\lambda_2-\lambda_3\right)]\\&-4p\left(4p^2-5p+2\right)\left(\cos\left(2\lambda_3\right)-i\sin\left(2\left(\lambda_1-\lambda_2\right)\right)\right)+8\left(4p^3-6p^2+3p-1\right)\\&\times[\cos\left(\lambda_1+\lambda_2-\lambda_3\right)+1]\}+2p^2\left(16p^4-40p^3+42p^2-22p+5\right)\{\alpha_1^2\alpha_2^2\cos[2\left(\lambda_1-\lambda_2\right)]\\&+\alpha_0^2\alpha_3^2\cos\left(2\lambda_3\right)\}+2p^2\left(16p^4-44p^3+50p^2-27p+6\right)\{\left(\alpha_0^2\alpha_2^2+\alpha_1^2\alpha_3^2\right)\cos\left(\lambda_1-\lambda_2-\lambda_3\right)\\&+\left(\alpha_0^2\alpha_1^2+\alpha_2^2\alpha_3^2\right)\cos\left(\lambda_1-\lambda_2+\lambda_3\right)\}+2\left(\alpha_1^2+\alpha_2^2\right)\left(\alpha_0^2+\alpha_3^2\right)\left(16p^4-20p^3+14p^2-5p+1\right)\\&\times(p-1)^2+2\left(\alpha_1^2\alpha_2^2+\alpha_0^2\alpha_3^2\right)\left(16p^4-24p^3+18p^2-6p+1\right)(p-1)^2-2\left(\alpha_1^2+\alpha_2^2\right)\left(\alpha_0^2+\alpha_3^2\right)\\&\times p\left(16p^5-44p^4+50p^3-31p^2+11p-2\right)\cos\left(\lambda_1+\lambda_2-\lambda_3\right)-8\left(\alpha_1^2\alpha_2^2+\alpha_0^2\alpha_3^2\right)\\&\times p\left(8p^5-24p^4+29p^3-18p^2+6p-1\right)\cos\left(\lambda_1-\lambda_2\right)\cos\left(\lambda_3\right)\\&+2p\left(16p^5-52p^4+70p^3-49p^2+18p-3\right)\{\alpha_0^2[\alpha_1^2\cos\left(2\lambda_1\right)+\alpha_2^2\cos\left(2\lambda_2\right)]\\&+\alpha_3^2[\alpha_1^2\cos\left(2\left(\lambda_1-\lambda_3\right)\right)+\alpha_2^2\cos\left(2\left(\lambda_2-\lambda_3\right)\right)]\}.\end{aligned}\tag{D11}$$

And using Eq. (D8), we obtain the corresponding average fidelity

$$F_{av}^B=1-\frac{1}{144}p\{-3\pi^2\left[p(8p-5)+2\right](p-1)^2-8p\left[p\left(4p\left(p\left(40p-133\right)+188\right)-601\right)+302\right]+728\}.\tag{D12}$$

(iii) Thirdly, we consider the case when every gate of the GHZ states preparation process is subjected to amplitude-damping noise. The Kraus operators take the form of

$$E_0=\begin{pmatrix}1&0\\0&\sqrt{1-p}\end{pmatrix},\qquad E_1=\begin{pmatrix}0&\sqrt{p}\\0&0\end{pmatrix}.\tag{D13}$$

Using a similar method as the above cases, the fidelity $F^A$ can be obtained as

$$\begin{aligned}F^A =&2\left(\alpha_1^2\alpha_2^2+\alpha_0^2\alpha_3^2\right)(p-1)^5\left(p^3-p^2-1\right)+\left(\alpha_0^4+\alpha_1^4+\alpha_2^4+\alpha_3^4\right)\left(p^4-3p^3+3p^2-p+1\right)^2\\&+\left(\alpha_1^2+\alpha_2^2\right)\left(\alpha_0^2+\alpha_3^2\right)(p-1)^2[-2p^6+8p^5+3\left(\sqrt{1-p}-4\right)p^4\\&+\left(8-10\sqrt{1-p}\right)p^3+\left(11\sqrt{1-p}-4\right)p^2-(1-p)^{5/2}(p-2)p\cos\left(\lambda_1+\lambda_2-\lambda_3\right)\\&+\left(2-4\sqrt{1-p}\right)p+2\sqrt{1-p}]+2\alpha_0\alpha_1\alpha_2\alpha_3\mathrm{e}^{-\mathrm{i}(\lambda_1+\lambda_2+\lambda_3)}\left(\mathrm{e}^{\mathrm{i}(\lambda_1+\lambda_2)}+\mathrm{e}^{\mathrm{i}\lambda_3}\right)^2p(1-p)^{11/2}.\end{aligned}\tag{D14}$$

The corresponding average fidelity can be calculated as

$$\begin{aligned}F_{av}^A =&\frac{1}{288}\{16\left(7\sqrt{1-p}+11\right)-p[-64p^7+384p^6+3\left(\pi^2\sqrt{1-p}-8\left(7\sqrt{1-p}+40\right)\right)p^5\\&+\left(-15\pi^2\sqrt{1-p}+896\sqrt{1-p}+1328\right)p^4+2\left(15\pi^2\sqrt{1-p}-952\sqrt{1-p}-672\right)p^3\\&+6\left(-5\pi^2\sqrt{1-p}+336\sqrt{1-p}+216\right)p^2+\left(15\pi^2\sqrt{1-p}-1176\sqrt{1-p}-976\right)p\\&+64\left(7\sqrt{1-p}+6\right)-3\pi^2\sqrt{1-p}]\}.\end{aligned}\tag{D15}$$

(iv) At last, we consider the case when every gate of the GHZ states preparation process is subjected to depolarizing noise. The Kraus operators take the form of

$$E_0=\sqrt{1-\frac{3p}{4}}I,\qquad E_1=\frac{\sqrt{p}}{2}\sigma_x,\qquad E_2=\frac{\sqrt{p}}{2}\sigma_y,\qquad E_3=\frac{\sqrt{p}}{2}\sigma_z.\tag{D16}$$

The fidelity $F^D$ can be obtained as

$$\begin{aligned}F^D =&\left(\alpha_1^2\alpha_2^2+\alpha_0^2\alpha_3^2\right)[\frac{1}{2}(p-2)^2p^2+2(p-1)^{10}]+\frac{1}{4}\left(\alpha_0^4+\alpha_1^4+\alpha_2^4+\alpha_3^4\right)\left(p^2-2p+2\right)^2\\&+\frac{1}{2}\left(\alpha_1^2+\alpha_2^2\right)\left(\alpha_0^2+\alpha_3^2\right)\{2p^2\left(p^2-2p+2\right)+(1-p)^5[-2p^3+\left(2p^2-5p+4\right)\\&\times p\cos\left(\lambda_1+\lambda_2-\lambda_3\right)+7p^2-8p+4]\}+2\alpha_0\alpha_1\alpha_2\alpha_3(p-2)p(p-1)^5\left(\cos\left(\lambda_1+\lambda_2-\lambda_3\right)+1\right).\end{aligned}\tag{D17}$$

The corresponding average fidelity can be calculated as

$$\begin{aligned}F_{av}^D =&\frac{1}{192}\pi^2(p-2)p(p-1)^5+\frac{1}{72}p\{p[p(p(p(p(p(2p(6(p-10)p+277)-1559)+2961)\\&-3962)+3784)-2555)+1183]-352\}+1.\end{aligned}\tag{D18}$$

Summarizing cases (i)–(iv), we find that $F^P$ and $F^A$ do not depend on the phase information of the initial state to be prepared, and it is easy to verify the four kinds of fidelities all equal to 1 in the absence of noise. The average fidelities of the JRSP protocol over $p$ under the influence of four typical kinds of noise environments are plotted in Figure D1. Moreover, for $p\rightarrow 1$, the fidelities $F_{av}^A$ and $F_{av}^D$ steadily approach $\frac{4}{9}$ and $\frac{1}{4}$, respectively.

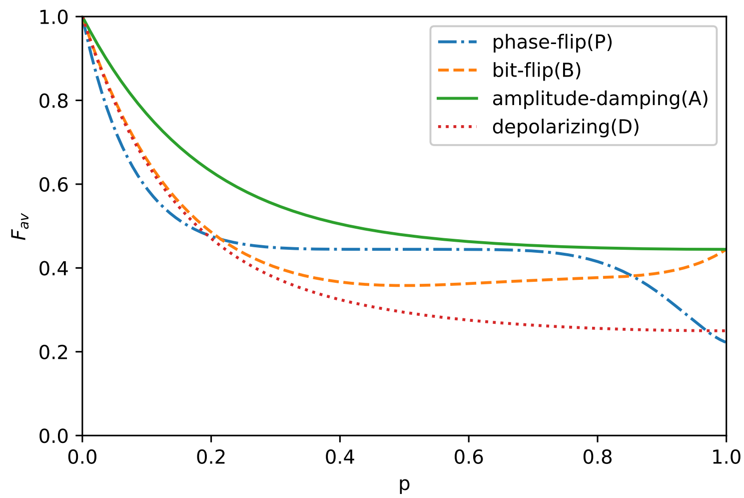


**Figure D1** (Color online) The average fidelities of JRSP of an arbitrary two-qubit state in four different noise environments are plotted as a function of $p$.

## Appendix E Experimental results and optimization of deterministic joint remote preparation of two unique two-qubit states in noise environments

In this appendix, we run our quantum circuit on the Origin NQVM, implementing the noises only on gates before the red dashed line in Figure B1. Without loss of generality, we consider remotely preparing the separated state $|\Psi_3\rangle$ and the maximally entangled state $|\Psi_5\rangle$ described in Eq. (C1),

$$\begin{aligned}|\Psi_3\rangle &= \frac{1}{2}(|0\rangle+|1\rangle)(|0\rangle+|1\rangle),\\ |\Psi_5\rangle &= \frac{1}{\sqrt{2}}(|00\rangle+|11\rangle),\end{aligned} \tag{E1}$$

which indicates the amplitude parameters $\alpha_0=\alpha_1=\alpha_2=\alpha_3=\frac{1}{2}$, and $\alpha_1=\alpha_2=0$, $\alpha_0=\alpha_3=\frac{1}{\sqrt{2}}$, respectively, and the phase parameters $\lambda_1=\lambda_2=\lambda_3=0$. The probability parameter $p$ we set goes from 0 to 1 in steps of 0.001. For each $p$, the NQVM runs 1000 times to calculate the experimental density matrix by quantum state tomography.

Using Eqs. (D7, D11, D14, D17), the theoretical fidelity $F_i^\gamma$ ($\gamma\in\{P,B,A,D\}$ and $i=3,5$ for the two states above) can be calculated as

$$\begin{aligned}
F_3^P &= \frac{1}{4}[1+(1-2p)^{10}+2(1-2p)^5],\\
F_5^P &= \frac{1}{2}(1+(1-2p)^{10}),\\
F_3^B &= 1,\\
F_5^B &= 1-4p+12p^2-16p^3+8p^4,\\
F_3^A &= \frac{1}{4}[1+2(1-p)^{5/2}+(1-p)^5],\\
F_5^A &= 1-\frac{7}{2}p+9p^2-14p^3+\frac{37}{2}p^4-\frac{41}{2}p^5+15p^6-6p^7+p^8,\\
F_3^D &= \frac{1}{4}[1-(1-p)^{10}+2(1-p)^5],\\
F_5^D &= \frac{1}{4}[2+2(1-p)^{10}-4p+6p^2-4p^3+p^4],
\end{aligned} \tag{E2}$$

respectively. How the state fidelities vary against $p$ in the four different types of noise environments are shown in Figures E1-E4, respectively.

From Figure E1, it can be seen that the experimental data is in good agreement with the theoretical fidelities under the influence of phase-flip noise. Moreover, it is also easy to verify that in the absence of phase-flip noise, all the fidelities are equal to 1. The state fidelity $F_3^P$ for JRSP of $|\Psi_3\rangle$ decreases as $p$ increases from zero, which is usual. However, for remotely preparing the state $|\Psi_5\rangle$, as $p$ increases further to the value larger than $\frac{1}{2}$, the protocol revives (i.e., back to service) with $F_5^P$ increasing, which seems unusual since it would mean that more noise better quality. These similar phenomena also happen in noisy quantum teleportation [71] and noisy JRSP of a single-qubit state [72]. Nevertheless, how can we improve the fidelity of our JRSP protocol, preventing the fidelity from falling to zero? In the presence of noises, the state working in channels is not the initial entangled resource but the decohered one. Specifically, when $p\neq 0$, the working state in

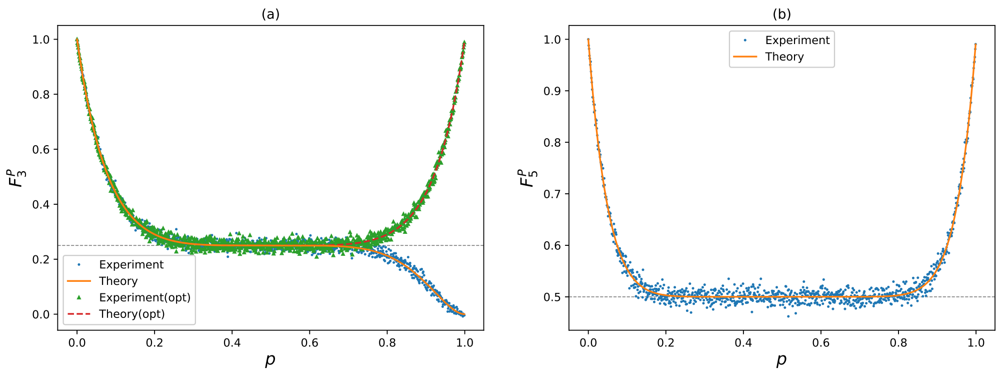


**Figure E1** (Color online) Fidelity of remotely preparing the state $|\Psi_3\rangle$ (a) and $|\Psi_5\rangle$ (b) in the phase-flip noise environment. The optimized theoretical $F_3^P$ for any $p$ are over 0.25.

our protocol may be the decohered state rather than GHZ states. Similar to the physical interpretations in Ref. [72], we consider the working state in our protocol to be the form of

$$\begin{aligned}|Q(\theta)\rangle_{024} &= (\cos\frac{\theta}{2}|000\rangle_{024} + \sin\frac{\theta}{2}|111\rangle_{024}),\\ |Q(\theta)\rangle_{135} &= (\cos\frac{\theta}{2}|000\rangle_{135} + \sin\frac{\theta}{2}|111\rangle_{135}).\end{aligned} \tag{E3}$$

In the following, let us see what Alice and Bob can do to improve the fidelity of different noises acting on the quantum channel. Since the ideal state $|Q(\pi/2)\rangle$ is maximally entangled, generally, the efficiency of the JRSP protocol will be enhanced as the $|Q(\theta)\rangle\langle Q(\theta)|$ approaches $|Q(\pi/2)\rangle\langle Q(\pi/2)|$. To investigate the validity of this idea, we conduct tests involving the remote preparation of the two initial states shown in Eq. (E1) under four distinct noise environments.

According to the Kraus operators described by Eq. (D5), the fidelities when considering the working state become

$$\begin{aligned}F_3'^P &= \frac{1}{4}[(1-2p)^{10}\sin^2(\theta) - 2(2p-1)^5\sin(\theta) + 1],\\ F_5'^P &= \frac{1}{2}[(1-2p)^{10}\sin^2(\theta) + 1].\end{aligned} \tag{E4}$$

The optimal value of $\theta$ that maximizes the fidelity can be determined from the equation $\frac{\partial F'}{\partial\theta} = 0$ and the restraint condition $\frac{\partial^2 F'}{\partial\theta^2} < 0$. For $F_3'^P$ and $F_5'^P$, the optimal values of $\theta$ are

$$\begin{aligned}\theta_3^P &= \begin{cases} \frac{\pi}{2}, & \text{for } p \leqslant \frac{1}{2}\\ -\frac{\pi}{2}, & \text{for } p > \frac{1}{2},\end{cases}\\ \theta_5^P &= \pm\frac{\pi}{2},\end{aligned} \tag{E5}$$

respectively. For remotely preparing state $|\Psi_3\rangle$, $|Q(\theta = -\pi/2)\rangle\langle Q(\theta = -\pi/2)|$ is closest to $\rho_{GHZ}$ when the probability parameter $p$ is larger than $\frac{1}{2}$. By choosing an appropriate $\theta$ for state $|Q(\theta)\rangle$, i.e. replacing the two Hadamard gates in Eq. (D2) with the parameterized unitary operation

$$U(\theta) = \begin{pmatrix}\cos\frac{\theta}{2} & \sin\frac{\theta}{2}\\ \sin\frac{\theta}{2} & -\cos\frac{\theta}{2}\end{pmatrix}, \tag{E6}$$

the entanglement degree contained in the working state enhances with the increase of $p$ ($> \frac{1}{2}$). After optimization, $F_3^P$ becomes

$$(F_3^P)_{opt} = \begin{cases}\frac{1}{4}[1 + (1-2p)^{10} + 2(1-2p)^5], & \text{for } p \leqslant \frac{1}{2}\\ \frac{1}{4}[1 + (1-2p)^{10} - 2(1-2p)^5], & \text{for } p > \frac{1}{2},\end{cases} \tag{E7}$$

which is shown in Figure E1, while $F_5^P$ can not be optimized.

Further, we consider the JRSP in the bit-flip noise environment. The optimal values of $\theta$ are found to be

$$\theta_3^B = \theta_5^B = \pm\frac{\pi}{2}. \tag{E8}$$

The original GHZ states in Eq. (B2) are one of the two optimal states, so the optimal fidelities are the same as $F_3^B$ and $F_5^B$ in Eq. (E2), respectively. It can be seen when implementing the JRSP of state $|\Psi_3\rangle$ in the bit-flip noise environment (Figure E2(a)), the fidelity is always unit for any $p$. That is to say, the bit-flip noise can not influence the JRSP of state $|\Psi_3\rangle$.

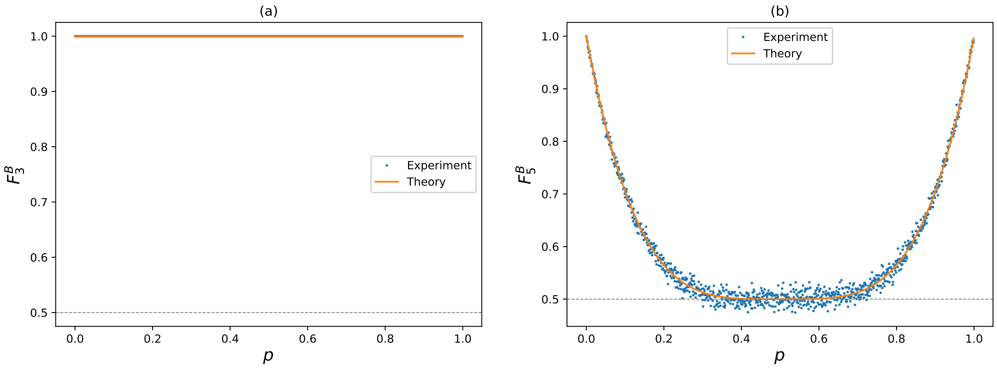


**Figure E2** (Color online) Fidelity of remotely preparing the state $|\Psi_3\rangle$ (a) and $|\Psi_5\rangle$ (b) in the bit-flip noise environment. Theoretical $F_3^B$ are always one, and theoretical $F_5^B$ are all over 0.5.

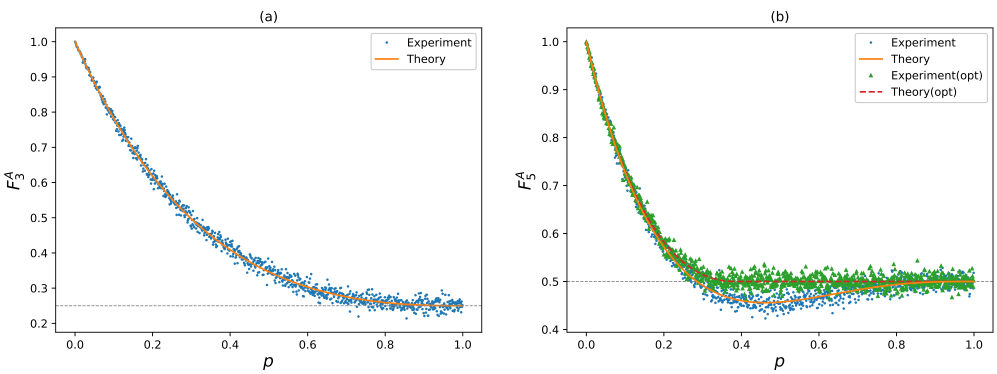


**Figure E3** (Color online) Fidelity of remotely preparing the state $|\Psi_3\rangle$ (a) and $|\Psi_5\rangle$ (b) in the amplitude-damping noise environment. Theoretical $F_3^A$ has a lower limit of 0.25, and the optimized theoretical $F_5^A$ are above 0.5.

And interestingly, for remotely preparing a maximally entangled state $|\Psi_5\rangle$, a complete revival (Figure E2(b)) happens in the bit-flip noise environment when $p \to 1$.

Affected by the amplitude-damping noise, the optimal values of $\theta$ are found to be

$$\begin{aligned} \theta_3^A &= \frac{\pi}{2}, \\ \theta_5^A &= \begin{cases} \pm 2\arctan\left(\sqrt{\dfrac{p^2-3p+1}{4p^5-12p^4+12p^3-3p^2-p+1}}\right), & \text{for } p \leqslant \dfrac{1}{2}\left(3-\sqrt{5}\right) \\ 0, \quad \text{for } p > \dfrac{1}{2}\left(3-\sqrt{5}\right). \end{cases} \end{aligned} \tag{E9}$$

The optimal average fidelity $(F_3^A)_{opt}$ is the same as $F_3^A$ in Eq. (E2) while $(F_5^A)_{opt}$ is different and derived as the form

$$(F_5^A)_{opt} = \begin{cases} \dfrac{2-p(p(p((p-7)p+15)-15)+7)}{4(p-1)p^2+2}, & \text{for } p \leqslant \dfrac{1}{2}\left(3-\sqrt{5}\right) \\ \dfrac{1}{2}, \quad \text{for } p > \dfrac{1}{2}\left(3-\sqrt{5}\right). \end{cases} \tag{E10}$$

The experimental result of the optimized JRSP of state $|\Psi_5\rangle$ in amplitude-damping noise environment derived from the Origin NQVM is shown in Figure E3. After optimization, we improve the fidelity $F_5^A$ all above $\frac{1}{2}$.

Finally, we consider the JRSP in the depolarizing noise environment. Straightforward calculations obtain the optimal values of $\theta$ as

$$\begin{aligned} \theta_3^D &= \frac{\pi}{2}, \\ \theta_5^D &= \pm\frac{\pi}{2}. \end{aligned} \tag{E11}$$

As displayed in Figure E4, the fidelities $F_3^D$ and $F_5^D$ decline when $p$ rises from 0 to 1, which our method cannot optimize.

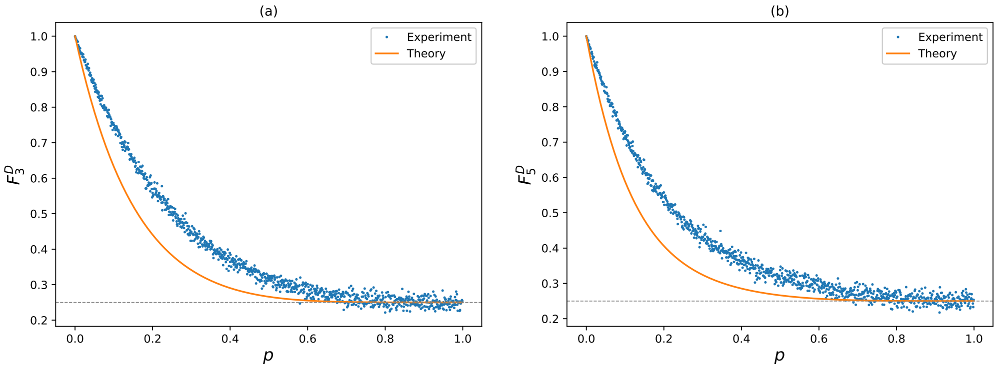


**Figure E4** (Color online) Fidelity of remotely preparing the state $|\Psi_3\rangle$ (a) and $|\Psi_5\rangle$ (b) in the depolarizing noise environment. Theoretical $F_3^D$ and $F_5^D$ are all above 0.25.

## Appendix F Conclusions

In summary, by employing two tripartite GHZ states as entanglement channels, we have realized the deterministic JRSP protocol of six unique initial two-qubit states on the Origin Wuyuan 6-qubit chip. The probability comparison between the simulator and real device, and the density matrices reconstructed by quantum state tomography, show that the protocol is successfully demonstrated on Origin Quantum Cloud, with all six experimental fidelities exceeding 0.4 —— the classical limit.

The effect of four kinds of noises on JRSP of any two-qubit pure state is investigated, and we have analytically derived the fidelity and their corresponding average one. Furthermore, for JRSP of a separated state and a maximally entangled state, the theoretical fidelities as a function of probability parameter $p$ are verified by the Origin NQVM. Especially for remotely preparing certain states in the presence of phase-flip and amplitude-damping noises, we have proposed a practical approach to enhance the fidelity by substituting the two Hadamard gates in the GHZ states preparation circuit with parameterized unitary operations. Simulated results on NQVM indicate that this approach can be implemented in the actual JRSP experiment. Our work proves the feasibility of JRSP of an arbitrary two-qubit state and could pave the way for developing and verifying more complex quantum communication tasks.

## Appendix G The density matrices and fidelities of the initial states

For each of the six initial states $|\Psi_1\rangle - |\Psi_6\rangle$, we run the Origin 6-qubit chip 10 times to calculate the mean fidelity. For simplicity, in the following, we present the theoretical density matrix and one of ten experimental density matrices of each state. Besides, ten experimental fidelities of each state are calculated accordingly.

(i) $|\Psi_1\rangle = |00\rangle$

$$\rho_1^T = \begin{pmatrix} 1 & 0 & 0 & 0 \\ 0 & 0 & 0 & 0 \\ 0 & 0 & 0 & 0 \\ 0 & 0 & 0 & 0 \end{pmatrix}, \tag{G1}$$

$$\rho_1^E = \begin{pmatrix} 0.7015 & -0.0043 & 0.0023 & -0.0056 \\ -0.0043 & 0.1227 & -0.0064 & -0.0015 \\ 0.0023 & -0.0064 & 0.1490 & 0.0086 \\ -0.0056 & -0.0015 & 0.0086 & 0.0269 \end{pmatrix} + \mathrm{i} \begin{pmatrix} 0 & 0.0119 & 0.0076 & -0.0005 \\ -0.0119 & 0 & -0.0104 & -0.0008 \\ -0.0076 & 0.0104 & 0 & 0.0025 \\ 0.0005 & 0.0008 & -0.0025 & 0 \end{pmatrix}. \tag{G2}$$

Here, the fidelity $F_1 = 0.70147$. The ten experimental fidelities are 0.69995, 0.695388, 0.652813, 0.689813, 0.690826, 0.70147, 0.698429, 0.694881, 0.699443, 0.69032.

(ii) $|\Psi_2\rangle = |11\rangle$

$$\rho_2^T = \begin{pmatrix} 0 & 0 & 0 & 0 \\ 0 & 0 & 0 & 0 \\ 0 & 0 & 0 & 0 \\ 0 & 0 & 0 & 1 \end{pmatrix}, \tag{G3}$$

$$\rho_2^E = \begin{pmatrix} 0.0335 & 0.0023 & 0.0058 & 0.0035 \\ 0.0023 & 0.1343 & -0.0079 & -0.0152 \\ 0.0058 & -0.0079 & 0.1272 & 0.0020 \\ 0.0035 & -0.0152 & 0.0020 & 0.7050 \end{pmatrix} + \mathrm{i} \begin{pmatrix} 0 & 0.0038 & 0.0063 & 0.0142 \\ -0.0038 & 0 & -0.0018 & -0.0010 \\ -0.0063 & 0.0018 & 0 & -0.0142 \\ -0.0142 & 0.0010 & 0.0142 & 0 \end{pmatrix}, \tag{G4}$$

the fidelity $F_2 = 0.705018$. Ten experimental fidelities are 0.69336, 0.695895, 0.68373, 0.608211, 0.694881, 0.692854, 0.705018, 0.690826, 0.615307, 0.696402.

(iii) $|\Psi_3\rangle = \frac{1}{2}(|0\rangle + |1\rangle)(|0\rangle + |1\rangle)$

$$\rho_3^T = \frac{1}{4}\begin{pmatrix} 1 & 1 & 1 & 1 \\ 1 & 1 & 1 & 1 \\ 1 & 1 & 1 & 1 \\ 1 & 1 & 1 & 1 \end{pmatrix}, \tag{G5}$$

$$\rho_3^E = \begin{pmatrix} 0.2458 & 0.1807 & 0.1338 & 0.0937 \\ 0.1807 & 0.2539 & 0.1001 & 0.1528 \\ 0.1338 & 0.1001 & 0.2696 & 0.1921 \\ 0.0937 & 0.1528 & 0.1921 & 0.2549 \end{pmatrix} + \mathrm{i}\begin{pmatrix} 0 & -0.0013 & -0.0010 & -0.0033 \\ 0.0013 & 0 & 0.0066 & -0.0008 \\ 0.0010 & -0.0066 & 0 & -0.0096 \\ 0.0033 & 0.0008 & 0.0096 & 0 \end{pmatrix}, \tag{G6}$$

the fidelity $F_3 = 0.676635$. Ten experimental fidelities are 0.674607, 0.648505, 0.656108, 0.674861, 0.669286, 0.651039, 0.66143, 0.676635, 0.651293, 0.667765.

(iv) $|\Psi_4\rangle = \frac{1}{2}(|0\rangle + \mathrm{i}|1\rangle)(|0\rangle + \mathrm{i}|1\rangle)$

$$\rho_4^T = \frac{1}{4}\begin{pmatrix} 1 & \mathrm{i} & \mathrm{i} & -1 \\ \mathrm{i} & -1 & -1 & -\mathrm{i} \\ \mathrm{i} & -1 & -1 & -\mathrm{i} \\ -1 & -\mathrm{i} & -\mathrm{i} & 1 \end{pmatrix}, \tag{G7}$$

$$\rho_4^E = \begin{pmatrix} 0.2387 & -0.0073 & -0.0020 & -0.0659 \\ -0.0073 & 0.2499 & 0.0793 & -0.0003 \\ -0.0020 & 0.0793 & 0.2676 & -0.0015 \\ -0.0659 & -0.0003 & -0.0015 & 0.2438 \end{pmatrix} + \mathrm{i}\begin{pmatrix} 0 & -0.1444 & -0.1217 & 0.0030 \\ 0.1444 & 0 & -0.0003 & -0.1113 \\ 0.1217 & 0.0003 & 0 & -0.1417 \\ -0.0030 & 0.1113 & 0.1417 & 0 \end{pmatrix}, \tag{G8}$$

the fidelity $F_4 = 0.58210$. Ten experimental fidelities are 0.575773, 0.570451, 0.544856, 0.578054, 0.581602, 0.582109, 0.574253, 0.575773, 0.579321, 0.581602.

(v) $|\Psi_5\rangle = \frac{1}{\sqrt{2}}(|00\rangle + |11\rangle)$

$$\rho_5^T = \frac{1}{2}\begin{pmatrix} 1 & 0 & 0 & 1 \\ 0 & 0 & 0 & 0 \\ 0 & 0 & 0 & 0 \\ 1 & 0 & 0 & 1 \end{pmatrix}, \tag{G9}$$

$$\rho_5^E = \begin{pmatrix} 0.3634 & 0.0043 & -0.0056 & 0.2126 \\ 0.0043 & 0.1485 & 0.0112 & 0.0094 \\ -0.0056 & 0.0112 & 0.1343 & 0.0015 \\ 0.2126 & 0.0094 & 0.0015 & 0.3538 \end{pmatrix} + \mathrm{i}\begin{pmatrix} 0 & -0.0038 & -0.0068 & -0.0086 \\ 0.0038 & 0 & -0.0023 & 0.0081 \\ 0.0068 & 0.0023 & 0 & -0.0142 \\ 0.0086 & -0.0081 & 0.0142 & 0 \end{pmatrix}, \tag{G10}$$

the fidelity $F_5 = 0.571214$. Ten experimental fidelities are 0.528386, 0.521543, 0.571214, 0.558036, 0.564118, 0.553475, 0.556262, 0.54866, 0.520783, 0.551447.

(vi) $|\Psi_6\rangle = \frac{1}{\sqrt{2}}(|01\rangle - |10\rangle)$

$$\rho^T = \frac{1}{2}\begin{pmatrix} 0 & 0 & 0 & 0 \\ 0 & 1 & -1 & 0 \\ 0 & -1 & 1 & 0 \\ 0 & 0 & 0 & 0 \end{pmatrix}, \tag{G11}$$

$$\rho_6^E = \begin{pmatrix} 0.1338 & 0.0069 & -0.0048 & -0.0051 \\ 0.0069 & 0.3492 & -0.1579 & 0.0051 \\ -0.0048 & -0.1579 & 0.3730 & 0.0021 \\ -0.0051 & 0.0051 & 0.0021 & 0.1439 \end{pmatrix} + \mathrm{i}\begin{pmatrix} 0 & -0.0053 & 0.0107 & -0.0028 \\ 0.0053 & 0 & 0.0015 & -0.0058 \\ -0.0107 & -0.0015 & 0 & 0.0010 \\ 0.0028 & 0.0058 & -0.0010 & 0 \end{pmatrix}, \tag{G12}$$

the fidelity $F_6 = 0.519009$. Ten experimental fidelities are 0.489612, 0.518756, 0.518756, 0.505578, 0.51242, 0.505324, 0.492907, 0.50127, 0.519009, 0.483277.

## Appendix H Density matrix of JRSP of an arbitrary two-qubit state in different noise environments

Here, we list the theoretical density matrix elements of JRSP of an arbitrary two-qubit state in different noise environments as follows.

(i) Bit-flip noise

In a similar calculation to the case of phase-flip noises, for the bit-flip noise environment, the density matrix elements of particles 4 and 5 are derived as

$$
\begin{aligned}
\rho_{00} &= \alpha_0^2\left(2p^2-2p+1\right)^2+4\alpha_3^2(p-1)^2p^2-2\left(\alpha_1^2+\alpha_2^2\right)(p-1)p\left(2p^2-2p+1\right),\\
\rho_{11} &= \alpha_1^2\left(2p^2-2p+1\right)^2+4\alpha_2^2(p-1)^2p^2-2\left(\alpha_0^2+\alpha_3^2\right)(p-1)p\left(2p^2-2p+1\right),\\
\rho_{22} &= 4\alpha_1^2(p-1)^2p^2+\alpha_2^2\left(2p^2-2p+1\right)^2-2\left(\alpha_0^2+\alpha_3^2\right)(p-1)p\left(2p^2-2p+1\right),\\
\rho_{33} &= 4\alpha_0^2(p-1)^2p^2+\alpha_3^2\left(2p^2-2p+1\right)^2-2\left(\alpha_1^2+\alpha_2^2\right)(p-1)p\left(2p^2-2p+1\right),\\
\rho_{10} &= \rho_{01}^* = \alpha_2\alpha_3(p-1)p\{-\mathrm{e}^{\mathrm{i}(\lambda_3-\lambda_2)}+2\mathrm{i}p\left(4p^2-6p+3\right)[\sin(\lambda_1)-\sin(\lambda_2-\lambda_3)]-e^{\mathrm{i}\lambda_1}\}\\
&\quad+\alpha_0\alpha_1\{e^{i(\lambda_2-\lambda_3)}p^2\left(16p^4-44p^3+50p^2-27p+6\right)+\left(16p^4-20p^3+14p^2-5p+1\right)\\
&\quad\times(p-1)^2e^{\mathrm{i}\lambda_1}-e^{i(\lambda_3-\lambda_2)}p\left(16p^5-44p^4+50p^3-31p^2+11p-2\right)\\
&\quad-p\left(16p^5-52p^4+70p^3-49p^2+18p-3\right)\mathrm{e}^{-\mathrm{i}\lambda_1}\},\\
\rho_{20} &= \rho_{02}^* = \alpha_1\alpha_3(p-1)p\{-\mathrm{e}^{\mathrm{i}(\lambda_3-\lambda_1)}+2\mathrm{i}p\left(4p^2-6p+3\right)[\sin(\lambda_2)-\sin(\lambda_1-\lambda_3)]-e^{\mathrm{i}\lambda_2}\}\\
&\quad+\alpha_0\alpha_2[\mathrm{e}^{\mathrm{i}\lambda_2}\left(16p^4-20p^3+14p^2-5p+1\right)(p-1)^2+\mathrm{e}^{\mathrm{i}(\lambda_1-\lambda_3)}p^2\\
&\quad\times\left(16p^4-44p^3+50p^2-27p+6\right)-\mathrm{e}^{\mathrm{i}(\lambda_3-\lambda_1)}p\left(16p^5-44p^4+50p^3-31p^2+11p-2\right)\\
&\quad-p\left(16p^5-52p^4+70p^3-49p^2+18p-3\right)\mathrm{e}^{-\mathrm{i}\lambda_2}],\\
\rho_{30} &= \rho_{03}^* = \alpha_1\alpha_2(p-1)p[2\left(-2p^2+2p-1\right)\cos(\lambda_1-\lambda_2)-2p\left(4p^2-5p+2\right)\mathrm{e}^{-\mathrm{i}\lambda_3}\\
&\quad+2\left(4p^3-7p^2+4p-1\right)\mathrm{e}^{\mathrm{i}\lambda_3}]+\alpha_0\alpha_3[\left(16p^4-24p^3+18p^2-6p+1\right)(p-1)^2e^{\mathrm{i}\lambda_3}\\
&\quad+p^2\left(16p^4-40p^3+42p^2-22p+5\right)\mathrm{e}^{-\mathrm{i}\lambda_3}\\
&\quad-4p\left(8p^5-24p^4+29p^3-18p^2+6p-1\right)\cos(\lambda_1-\lambda_2)],\\
\rho_{21} &= \rho_{12}^* = \alpha_0\alpha_3(p-1)p[-2\mathrm{e}^{\mathrm{i}(\lambda_1-\lambda_2)}p\left(4p^2-5p+2\right)+2\left(-2p^2+2p-1\right)\cos(\lambda_3)\\
&\quad+2\mathrm{e}^{\mathrm{i}(\lambda_2-\lambda_1)}\left(4p^3-7p^2+4p-1\right)]+\alpha_1\alpha_2[\mathrm{e}^{\mathrm{i}(\lambda_2-\lambda_1)}\left(16p^4-24p^3+18p^2-6p+1\right)(p-1)^2\\
&\quad+\mathrm{e}^{\mathrm{i}(\lambda_1-\lambda_2)}p^2\left(16p^4-40p^3+42p^2-22p+5\right)-2p\left(8p^5-24p^4+29p^3-18p^2+6p-1\right)\\
&\quad\times\mathrm{e}^{-\mathrm{i}\lambda_3}-2p\left(8p^5-24p^4+29p^3-18p^2+6p-1\right)e^{\mathrm{i}\lambda_3}],\\
\rho_{31} &= \rho_{13}^* = \alpha_0\alpha_2(p-1)p\{-\mathrm{e}^{\mathrm{i}(\lambda_3-\lambda_1)}+2\mathrm{i}p\left(4p^2-6p+3\right)[\sin(\lambda_2)-\sin(\lambda_1-\lambda_3)]-e^{\mathrm{i}\lambda_2}\}\\
&\quad+\alpha_1\alpha_3[\mathrm{e}^{\mathrm{i}(\lambda_3-\lambda_1)}\left(16p^4-20p^3+14p^2-5p+1\right)(p-1)^2+p^2\left(16p^4-44p^3+50p^2-27p+6\right)\\
&\quad\times e^{-\mathrm{i}\lambda_2}-\mathrm{e}^{\mathrm{i}(\lambda_1-\lambda_3)}p\left(16p^5-52p^4+70p^3-49p^2+18p-3\right)\\
&\quad-p\left(16p^5-44p^4+50p^3-31p^2+11p-2\right)\mathrm{e}^{\mathrm{i}\lambda_2}],\\
\rho_{32} &= \rho_{23}^* = \alpha_0\alpha_1(p-1)p\{-\mathrm{e}^{\mathrm{i}(\lambda_3-\lambda_2)}+2\mathrm{i}p\left(4p^2-6p+3\right)[\sin(\lambda_1)-\sin(\lambda_2-\lambda_3)]-\mathrm{e}^{\mathrm{i}\lambda_1}\}\\
&\quad+\alpha_2\alpha_3[\mathrm{e}^{\mathrm{i}(\lambda_3-\lambda_2)}\left(16p^4-20p^3+14p^2-5p+1\right)(p-1)^2\\
&\quad+p^2\left(16p^4-44p^3+50p^2-27p+6\right)\mathrm{e}^{-\mathrm{i}\lambda_1}-\mathrm{e}^{\mathrm{i}(\lambda_2-\lambda_3)}p\left(16p^5-52p^4+70p^3-49p^2+18p-3\right)\\
&\quad-p\left(16p^5-44p^4+50p^3-31p^2+11p-2\right)\mathrm{e}^{\mathrm{i}\lambda_1}].
\end{aligned}
\tag{H1}
$$

(ii) Amplitude-damping noise

For the amplitude-damping noise environment, the density matrix elements of particles 4 and 5 are derived as

$$\begin{aligned}
\rho_{00} &= \alpha_3^2 p^2(1-p)^6 + \alpha_0^2\left(p(p-1)^3+1\right)^2 + \left(\alpha_1^2+\alpha_2^2\right)(1-p)^3 p\left(p(p-1)^3+1\right),\\
\rho_{11} &= \alpha_2^2 p^2(1-p)^6 + \alpha_1^2\left(p(p-1)^3+1\right)^2 + \left(\alpha_0^2+\alpha_3^2\right)(1-p)^3 p\left(p(p-1)^3+1\right),\\
\rho_{22} &= \alpha_1^2 p^2(1-p)^6 + \alpha_2^2\left(p(p-1)^3+1\right)^2 + \left(\alpha_0^2+\alpha_3^2\right)(1-p)^3 p\left(p(p-1)^3+1\right),\\
\rho_{33} &= \alpha_0^2 p^2(1-p)^6 + \alpha_3^2\left(p(p-1)^3+1\right)^2 + \left(\alpha_1^2+\alpha_2^2\right)(1-p)^3 p\left(p(p-1)^3+1\right),\\
\rho_{01} &= \rho_{10}^* = \frac{1}{2}(1-p)^{5/2}\{\alpha_0\alpha_1[e^{-i\lambda_1}\left(p(3p-4)(p-1)^2+2\right) - \mathrm{e}^{\mathrm{i}(\lambda_2-\lambda_3)}(p-2)(p-1)^2 p]\\
&\quad - \alpha_2\alpha_3\left(\mathrm{e}^{-\mathrm{i}\lambda_1}+\mathrm{e}^{\mathrm{i}(\lambda_2-\lambda_3)}\right)(p-1)^3 p\},\\
\rho_{02} &= \rho_{20}^* = \frac{1}{2}(1-p)^{5/2}\{\alpha_0\alpha_2[\mathrm{e}^{-\mathrm{i}\lambda_2}\left(p(3p-4)(p-1)^2+2\right) - \mathrm{e}^{\mathrm{i}(\lambda_1-\lambda_3)}(p-2)(p-1)^2 p]\\
&\quad - \alpha_1\alpha_3\left(\mathrm{e}^{-\mathrm{i}\lambda_2}+\mathrm{e}^{\mathrm{i}(\lambda_1-\lambda_3)}\right)(p-1)^3 p\},\\
\rho_{03} &= \rho_{30}^* = \alpha_0\alpha_3\mathrm{e}^{-\mathrm{i}\lambda_3}(1-p)^5,\\
\rho_{12} &= \rho_{21}^* = \alpha_1^2 + p(p-1)^3\left(2\alpha_1^2-\alpha_3^2+\left(\alpha_1^2+\alpha_2^2-\alpha_3^2\right)p(p-1)^3+\alpha_0^2\left(-p(p-1)^3-1\right)\right),\\
\rho_{13} &= \rho_{31}^* = \alpha_1\alpha_2\mathrm{e}^{\mathrm{i}(\lambda_1-\lambda_2)}(1-p)^5,\\
\rho_{23} &= \rho_{32}^* = \frac{1}{2}(1-p)^{5/2}\{\alpha_2\alpha_3[\mathrm{e}^{\mathrm{i}(\lambda_2-\lambda_3)}\left(p(3p-4)(p-1)^2+2\right) - \mathrm{e}^{-\mathrm{i}\lambda_1}(p-2)(p-1)^2 p]\\
&\quad - \alpha_0\alpha_1\left(\mathrm{e}^{-\mathrm{i}\lambda_1}+\mathrm{e}^{\mathrm{i}(\lambda_2-\lambda_3)}\right)(p-1)^3 p\}.
\end{aligned} \tag{H2}$$

(iii) Depolarizing noise

For the depolarizing noise environment, the density matrix elements of particles 4 and 5 are derived as

$$\begin{aligned}
\rho_{00} &= \frac{1}{4}\left(\alpha_0^2\left(p^2-2p+2\right)^2+\alpha_3^2(p-2)^2p^2+\left(\alpha_1^2+\alpha_2^2\right)(2-p)p\left(p^2-2p+2\right)\right),\\
\rho_{11} &= \frac{1}{4}\left(\alpha_1^2\left(p^2-2p+2\right)^2+\alpha_2^2(p-2)^2p^2+\left(\alpha_0^2+\alpha_3^2\right)(2-p)p\left(p^2-2p+2\right)\right),\\
\rho_{22} &= \frac{1}{4}\left(\alpha_1^2(p-2)^2p^2+\alpha_2^2\left(p^2-2p+2\right)^2+\left(\alpha_0^2+\alpha_3^2\right)(2-p)p\left(p^2-2p+2\right)\right),\\
\rho_{33} &= \frac{1}{4}\left(\alpha_0^2(p-2)^2p^2+\alpha_3^2\left(p^2-2p+2\right)^2+\left(\alpha_1^2+\alpha_2^2\right)(2-p)p\left(p^2-2p+2\right)\right),\\
\rho_{01} &= \rho_{10}^* = \frac{1}{4}(p-1)^5\{\alpha_0\alpha_1\left(\mathrm{e}^{-\mathrm{i}\lambda_1}(p-2)(p(2p-3)+2)-\mathrm{e}^{\mathrm{i}(\lambda_2-\lambda_3)}p(p(2p-5)+4)\right)\\
&\quad + \alpha_2\alpha_3\left(\mathrm{e}^{-\mathrm{i}\lambda_1}+\mathrm{e}^{\mathrm{i}(\lambda_2-\lambda_3)}\right)(p-2)p\},\\
\rho_{02} &= \rho_{20}^* = \frac{1}{4}(p-1)^5\{\alpha_0\alpha_2\left(\mathrm{e}^{-\mathrm{i}\lambda_2}(p-2)(p(2p-3)+2)-\mathrm{e}^{\mathrm{i}(\lambda_2-\lambda_3)}p(p(2p-5)+4)\right)\\
&\quad + \alpha_1\alpha_3\left(\mathrm{e}^{-\mathrm{i}\lambda_2}+\mathrm{e}^{\mathrm{i}(\lambda_1-\lambda_3)}\right)(p-2)p\},\\
\rho_{03} &= \rho_{30}^* = \alpha_0\alpha_3\mathrm{e}^{-\mathrm{i}\lambda_3}(p-1)^{10},\\
\rho_{12} &= \rho_{21}^* = \alpha_1\alpha_2\mathrm{e}^{\mathrm{i}(\lambda_1-\lambda_2)}(p-1)^{10},\\
\rho_{13} &= \rho_{31}^* = \frac{1}{4}(p-1)^5\{\alpha_0\alpha_2\left(\mathrm{e}^{-\mathrm{i}\lambda_2}+\mathrm{e}^{\mathrm{i}(\lambda_1-\lambda_3)}\right)(p-2)p\\
&\quad + \alpha_1\alpha_3\left(\mathrm{e}^{-\mathrm{i}\lambda_2}p((5-2p)p-4)+\mathrm{e}^{\mathrm{i}(\lambda_1-\lambda_3)}(p-2)(p(2p-3)+2)\right)\},\\
\rho_{23} &= \rho_{32}^* = \frac{1}{4}(p-1)^5\{\alpha_0\alpha_1\left(\mathrm{e}^{-\mathrm{i}\lambda_1}+\mathrm{e}^{\mathrm{i}(\lambda_2-\lambda_3)}\right)(p-2)p\\
&\quad + \alpha_2\alpha_3\left(\mathrm{e}^{-\mathrm{i}\lambda_1}p((5-2p)p-4)+\mathrm{e}^{\mathrm{i}(\lambda_1-\lambda_3)}(p-2)(p(2p-3)+2)\right)\}.
\end{aligned} \tag{H3}$$

## References


1 Bennett C H, Brassard G, Crepeau C, et al. Teleporting an unknown quantum state via dual classical and Einstein-Podolsky-Rosen channels. Phys Rev Lett, 1993, 70: 1895-1899

2 Lo H K. Classical-communication cost in distributed quantum-information processing: a generalization of quantum-communication complexity. Phys Rev A, 2000, 62: 012313

3 Pati A K. Minimum classical bit for remote preparation and measurement of a qubit. Phys Rev A, 2000, 63: 014302

4 Bennett C H, DiVincenzo D P, Shor P W, et al. Remote state preparation. Phys Rev Lett, 2001, 87: 077902

5 Devetak I, Berger T. Low-entanglement remote state preparation. Phys Rev Lett, 2001, 87: 197901

6 Leung D W, Shor P W. Oblivious remote state preparation. Phys Rev Lett, 2003, 90: 127905

7 Berry D W, Sanders B C. Optimal remote state preparation. Phys Rev Lett, 2003, 90: 057901

8 Solis-Prosser M A, Neves L. Remote state preparation of spatial qubits. Phys Rev A, 2011, 84: 012330

9 Zeng B, Zhang P. Remote-state preparation in higher dimension and the parallelizable manifold $S^{n-1}$. Phys Rev A, 2002, 65: 022316

10 Liu J M, and Wang Y Z. Remote preparation of a two-particle entangled state. Phys Lett A, 2003, 316: 159-167

11 Ye M Y, Zhang Y S, Guo G C. Faithful remote state preparation using finite classical bits and a nonmaximally entangled state. Phys Rev A, 2004, 69: 022310

12 Liu J M, Feng X L, Oh C H. Remote preparation of arbitrary two-and three-qubit states. EPL, 2009, 87: 30006

13 Daki B, Lipp Y O, Ma X, et al. Quantum discord as resource for remote state preparation. Nat Phys, 2012, 8: 666-670

14 Peng X H, Zhu X Z, Fang X M, et al. Experimental implementation of remote state preparation by nuclear magnetic resonance. Phys Lett A, 2003, 306: 271-276.

15 Xiang G Y, Li J, Yu B, et al. Remote preparation of mixed states via noisy entanglement. Phys Rev A, 2005, 72: 012315.

16 Rosenfeld W, Berner S, Volz J, et al. Remote preparation of an atomic quantum memory. Phys Rev Lett, 2007, 98: 050504.

17 Mikami H, Kobayashi T. Remote preparation of qutrit states with biphotons. Phys Rev A, 2007, 75: 022325

18 Killoran N, Biggerstaff D N, Kaltenbaek R, et al. Derivation and experimental test of fidelity benchmarks for remote preparation of arbitrary qubit states. Phys Rev A, 2010, 81: 012334.

19 Barreiro J T, Wei T C, Kwiat P G. Remote preparation of single-photon "hybrid" entangled and vector-polarization states. Phys Rev Lett, 2010, 105: 030407

20 Wu W, Liu W T, Chen P X, et al. Deterministic remote preparation of pure and mixed polarization states. Phys Rev A, 2010, 81: 042301

21 Pogorzalek S, Fedorov K G, Xu M, et al. Secure quantum remote state preparation of squeezed microwave states. Nat Commun, 2019, 10: 2604

22 Haffner T, Zanin G L, Gomes R M, et al. Remote preparation of single photon vortex thermal states. Eur Phys J Plus, 2020, 135: 601

23 Cameron A R, Cheng S W, Schwarz S, et al. Remote state preparation of single-photon orbital-angular-momentum lattices. Phys Rev A, 2021, 104: L051701

24 Kurucz Z, Adam P, Kis Z, et al. Continuous variable remote state preparation. Phys Rev A, 2005, 72: 052315

25 Le Jeannic H, Cavailles A, Raskop J, et al. Remote preparation of continuous-variable qubits using loss-tolerant hybrid entanglement of light. Optica, 2018, 5: 1012-1015

26 Liu S H, Han D M, Wang N, et al. Experimental demonstration of remotely creating Wigner negativity via quantum steering. Phys Rev Lett, 2022, 128: 200401

27 Han D M, Sun F X, Wang N, et al. Remote preparation of optical cat states based on Gaussian entanglement. Laser Photonics Rev, 2023, 17: 2300103

28 Xia Y, Song J, Song H S. Multiparty remote state preparation. J Phys B-At Mol Opt Phys, 2007, 40: 3719-3724

29 An N B, Kim J. Joint remote state preparation. J Phys B-At Mol Opt Phys, 2008, 41: 095501

30 An N B. Joint remote preparation of a general two-qubit state. J Phys B-At Mol Opt Phys, 2009, 42: 125501

31 An N B, Bich C T, Don N V. Deterministic joint remote state preparation. Phys Lett A, 2011, 375: 3570-3573

32 Hou K, Li Y B, Liu G H, et al. Joint remote preparation of an arbitrary two-qubit state via GHZ-type states. J Phys A-Math Theor, 2011, 44: 255304

33 Radmark M, Wiesniak M, Zukowski M, et al. Experimental multilocation remote state preparation. Phys Rev A, 2013, 88: 032304

34 Wang D, Ye L. Multiparty-controlled joint remote state preparation. Quantum Inf Process, 2013, 12: 3223-3237

35 Xiao X Q, Liu J M, Zeng G. Joint remote state preparation of arbitrary two-and three-qubit states. J Phys B-At Mol Opt Phys, 2011, 44: 075501

36 Chen Q Q, Xia Y, Song J, et al. Joint remote state preparation of a W-type state via W-type states. Phys Lett A, 2010, 374: 4483-4487

37 Luo M X, Chen X B, Ma S Y, et al. Joint remote preparation of an arbitrary three-qubit state. Opt Commun, 2010, 283: 4796-4801

38 Xia Y, Chen Q Q, An N B. Deterministic joint remote preparation of an arbitrary three-qubit state via Einstein-Podolsky-Rosen pairs with a passive receiver. J Phys A-Math Theor, 2012, 45: 335306

39 Zhan Y B, Hu B L, Ma P C. Joint remote preparation of four-qubit cluster-type states. J Phys B-At Mol Opt Phys, 2011, 44: 095501

40 Wang D, Hu Y D, Wang Z Q, et al. Efficient and faithful remote preparation of arbitrary three- and four-particle W-class entangled states. Quantum Inf Process, 2015, 14: 2135-2151

41 Zhou P. Joint remote preparation of an arbitrary m-qudit state with a pure entangled quantum channel via positive operator-valued measurement. J Phys A-Math Theor, 2012, 45: 215305

42 Wang D, Huang A J, Sun W Y, et al. Practical single-photon-assisted remote state preparation with non-maximally entanglement. Quantum Inf Process, 2016, 15: 3367-3381

43 Chen Z F, Liu J M, Ma L. Deterministic joint remote preparation of an arbitrary two-qubit state in the presence of noise. Chin Phys B, 2014, 23: 020312

44 Li J F, Liu J M, Feng X L, et al. Deterministic remote two-qubit state preparation in dissipative environments. Quantum Inf Process, 2016, 15: 2155-2168

45 Gu J R, Liu J M. Deterministic controlled bidirectional remote state preparation in dissipative environments. Commun Theor Phys, 2022, 74: 075101

46 Nielsen M A, Chuang I. Quantum Computation and Quantum Information. Cambridge: Cambridge University Press, 2002.
47 Wang M M, Qu Z G. Effect of quantum noise on deterministic joint remote state preparation of a qubit state via a GHZ channel. Quantum Inf Process, 2016, 15: 4805-4818
48 Qian Y J, Xue S B, Jiang M. Deterministic remote preparation of arbitrary single-qubit state via one intermediate node in noisy environment. Phys Lett A, 2020, 384: 126204
49 Adepoju A G, Falaye B J, Sun G H, et al. Joint remote state preparation (JRSP) of two-qubit equatorial state in quantum noisy channels. Phys Lett A, 2017, 381: 581-587
50 Wang M M, Qu Z G, Wang W, et al. Effect of noise on deterministic joint remote preparation of an arbitrary two-qubit state. Quantum Inf Process, 2017, 16: 140
51 Dash T, Sk R, Panigrahi P K. Deterministic joint remote state preparation of arbitrary two-qubit state through noisy cluster-GHZ channel. Opt Commun, 2020, 464: 125518
52 Hou K, Chen Z Y, Shi M, et al. Effective deterministic joint remote preparation of the Knill-Laflamme-Milburn state in collective noise environment. Quantum Inf Process, 2021, 20: 225
53 Zhang Z, Zhao C, Wang J, et al. Joint remote state preparation of mixed states. J Phys B-At Mol Opt Phys, 2020, 53: 025501
54 Kumar A, Haddadi S, Pourkarimi M R, et al. Experimental realization of controlled quantum teleportation of arbitrary qubit states via cluster states. Sci Rep, 2020, 10: 13608
55 Haddadi S, Hu M L, Khedif Y, et al. Measurement uncertainty and dense coding in a two-qubit system: Combined effects of bosonic reservoir and dipole-dipole interaction. Results Phys, 2022, 32: 105041
56 Vuillot C. Is error detection helpful on IBM 5Q chips? 2017, ArXiv:1705.08957
57 Willsch D, Willsch M, Jin F, et al. Testing quantum fault tolerance on small systems. Phys Rev A, 2018, 98: 052348
58 Harper R, Flammia S T. Fault-tolerant logical gates in the IBM quantum experience. Phys Rev Lett, 2019, 122: 080504
59 Li M, Shang Y. Entangled state generation via quantum walks with multiple coins. npj Quantum Inform, 2021, 7: 70
60 Chen C T, Shi Y H, Xiang Z, et al. ScQ cloud quantum computation for generating Greenberger-Horne-Zeilinger states of up to 10 qubits. Sci China Phys Mech Astron, 2022, 65: 110362
61 Liu S S, Li Y N, Duan R Y. Distinguishing unitary gates on the IBM quantum processor. Sci China Inform Sci, 2019, 62: 072502
62 Lamm H, Lawrence S. Simulation of nonequilibrium dynamics on a quantum computer. Phys Rev Lett, 2018, 121: 170501
63 Shang Y, Li M. Experimental realization of state transfer by quantum walks with two coins. Quantum Sci Technol, 2019, 5: 015005
64 Mei F, Guo Q, Yu Y F, et al. Digital simulation of topological matter on programmable quantum processors. Phys Rev Lett, 2020, 125: 160503
65 Motta M, Sun C, Tan A T, et al. Determining eigenstates and thermal states on a quantum computer using quantum imaginary time evolution. Nat Phys, 2020, 16: 205-210
66 Banerjee S, Mukherjee A, Panigrahi P K. Quantum blockchain using weighted hypergraph states. Phys Rev Res, 2020, 2: 013322
67 Karalekas P J, Tezak N A, Peterson E C, et al. A quantum-classical cloud platform optimized for variational hybrid algorithms. Quantum Sci Technol, 2020, 5: 024003
68 Zheng Q L, Zhu P Y, Xue S C, et al. Quantum algorithm and experimental demonstration for the subset sum problem. Sci China Inform Sci, 2022, 65: 182501
69 Wang X L, Cai X D, Su Z E, et al. Quantum teleportation of multiple degrees of freedom of a single photon. Nature, 2015, 518: 516-519
70 Hayashi A, Hashimoto T, Horibe M. Reexamination of optimal quantum state estimation of pure states. Phys Rev A, 2005, 72: 032325
71 Fortes R, Rigolin G. Fighting noise with noise in realistic quantum teleportation. Phys Rev A, 2015, 92: 012338
72 Nguyen V H, Cao T B, Nguyen B A. Optimal joint remote state preparation in the presence of various types of noises. Adv Nat Sci-Nanosci Nanotechnol, 2017, 8: 015012